

# Estimation of Hydraulic Conditions of Tsunami from Deposits by Inverse model using Deep Learning Neural Network

Rimali Mitra<sup>1</sup>, Hajime Naruse<sup>1</sup>

<sup>1</sup>Division of Earth and Planetary Sciences, Graduate School of Science, Kyoto University, Kitashirakawa Oiwakecho, Kyoto, Japan.

## Key Points:

- The inverse modeling for paleo-tsunami deposits was performed by using deep learning neural network
- Flow velocity, maximum flow depth, maximum inundation length, and sediment concentration of tsunamis of 2011 Tohoku-Oki Tsunami were quantitatively assessed by the established inverse model
- Comparison with observation and uncertainty analysis implied that the reconstructed flow conditions were accurate and reasonably precise.

---

Corresponding author: Rimali Mitra, [mitra.rimali.37z@st.kyoto-u.ac.jp](mailto:mitra.rimali.37z@st.kyoto-u.ac.jp)

## Abstract

Tsunami deposits provide clues to estimate magnitude and flow conditions of paleo-tsunamis, and numerical inverse model has decent potential to predict hydraulic conditions of tsunamis from their deposits. There are different kinds of inverse models proposed so far for tsunamis but most of them are based on oversimplified assumptions and share the limitation of applicability in original tsunami hydrodynamics with transportation and deposition settings. Here, we propose a new inverse model which serves as the modified version of previously proposed FITTNUSS model which incorporates nonuniform and unsteady transport of suspended sediment and turbulent mixing. The present model uses deep learning neural networks (DNN) as a technique for inversion method. In this method, forward model calculation was repeated at random initial flow conditions to produce artificial training data sets which represent depositional characteristics such as thickness and grain-size distribution. After that, DNN was trained for establishing the general inverse model, based on artificial data sets which were derived from the forward model. Tests using independent artificial data sets successfully indicated that the established DNN can reconstruct the original flow conditions from the characteristics of deposits. Finally, the model was applied to a data set of 2011 Tohoku-Oki Tsunami deposits around . Jackknife resampling has been applied for estimating the precision of the result. The estimated result of flow velocity was around 5.4 m/sec with  $\pm 0.140$  m after uncertainty analysis. The simulated result for maximum flow depth was around 4.11 m with  $\pm 0.152$  m. The DNN showed promising result for reconstruction from natural data set of the event which helps to estimate hydraulic conditions of paleo-tsunami based on realistic settings of tsunami deposits.

## Plain Language Summary

This study involves inverse modeling using artificial intelligence technique which helps to estimate hydraulic conditions of paleo-tsunami based on realistic settings of tsunami deposits.

## 1 Introduction

Tsunami is one of the most disastrous natural hazards along coastal zones. It is a threat to overall socio-economic infrastructure of coastal based cities (Lin et al., 2012). Tsunami hazard assessment is extremely necessary for any fast-growing coastal city. 2004

Indian Ocean Tsunami and 2011 Tohoku-Oki Tsunami caused devastating damage to many Asian countries and Japan but the situation gets worse when the countries lack tsunami related disaster preparedness that causes human causalities and building damages (Imamura et al., 2019). Ghobarah et al. (2006) reported that debris carried by 2004 Indian Ocean tsunami can cause major building damage. 2004 Indian Ocean Tsunami caused extensive structural and non-structural destruction of reinforced concrete buildings (Saatcioglu et al., 2005).

To mitigate tsunami disasters, inverse modeling of tsunamis from their geologic records has been developed. Tsunami deposits are defined as layers of sediment formed by hydrodynamic activities of tsunami, and the research of tsunami deposits has been started since early 1950s (Macdonald & Cox, 1950; Sugawara et al., 2014; Tang & Weiss, 2015). The mode of sediment transportation and deposition by tsunamis can be perceived by detailed study of tsunami deposits (Costa et al., 2015). Using these knowledges, quantitative reconstruction of environmental conditions such as flow velocity and maximum flow depth, has been attempted using several inverse modeling approaches (Johnson et al., 2017; Jerolmack & Paola, 2010; Ganti et al., 2014).

However, previous studies of inverse modeling were based on the forward models using unreasonably simplified assumptions. For example, settling-advection model (or moving settling tube model) assumes that all sediment particles settle in water column without any turbulent mixing, resuspension or erosional processes (Soulsby et al., 2007; Moore et al., 2007; B. E. Jaffe & Gelfenbaum, 2007). Tang and Weiss (2015) assumed that suspension in tsunamis are in uniform and steady conditions and inundation flows suddenly stop. As a result, situations that are suitable for their inverse models are quite limited (B. Jaffe et al., 2016; Naruse & Abe, 2017). Moore et al. (2007) proposed the point inverse model based on advection settings, where settling velocities of the larger particles (D<sub>84</sub> and D<sub>100</sub>) in the deposit were used as input data and the model estimated flow speed of the tsunami inundation. However, travel distances of the grains were largely underestimated in this model because of lack of resuspension processes. D. Smith et al. (2007) proposed another point model based on particle settling but only finest grain size classes 106-184  $\mu\text{m}$  were used in this model where incorporation of larger grain size classes are essential for accurate estimation from tsunami deposits (Naruse & Abe, 2017). On the other hand, Soulsby et al. (2007) proposed the 1-D model that deciphered run-up elevation and inundation distance, despite that in that model no resuspension, sediment

dynamics of optimization of input parameters were considered. B. E. Jaffe and Gelfenbuam (2007) proposed a point model (TsuSedMod) using suspended load as formulation (Madsen et al., 1993) to reconstruct maximum tsunami flow speed and vertical grain size distribution but temporal variation of deceleration of the flow was not considered. This model overestimated tsunami flow speed with uniform steady flow consideration in the formulations. Finally, FITTNUSS model (Naruse & Abe, 2017) solved most of the limitations of the previous models with using machine learning techniques. This model incorporates nonuniform and unsteady transport of suspended sediment and turbulent mixing; however, there were still many limitations of FITTNUSS model. It employed tedious trial and error method technique (L-BFGS-B method), which is less efficient optimization methods. As a result, it was difficult to deal with larger amount of data sets, and no uncertainty analysis was possible because computational statistical methods such as jackknife method requires iteration of inverse analysis.

To this end, in this study we propose a new inversion method which uses the deep-learning artificial neural network (DNN) (Romano et al., 2009) to implement the inverse model. This inverse model incorporates the same forward model used in FITTNUSS (Naruse and Abe, 2017). In this new methodology, however, initial conditions and model parameters of the forward model are not optimized to fit the observed characteristics of tsunami deposits. Instead, the forward model calculation was simply repeated at random initial flow conditions (e.g. maximum inundation length, maximum flow depth, flow velocity, concentration, etc.) to produce artificial training data sets which represent artificial depositional characteristics such as spatial distribution of thickness and grain-size composition. Then, DNN was trained for establishing the relation between characteristics of deposits and flow conditions based on artificial data sets. The established DNN can instantaneously predict the probable flow conditions from deposits, so that it works as the inverse model of tsunami deposits. The performance of the model was checked using training and test data set. The verification of efficiency of the model using data set showed good results. Finally, this 1-D model has been applied to 2011 Tohoku-Oki Tsunami deposits which around Sendai plain and fair prediction of flow velocity, maximum flow depth, concentration of six grain size classes were obtained. The precision of the paleo hydraulics was also checked by jackknife method. The methodology and result were compared with the FITTNUSS model and actual initial flow conditions. The comparison shows promising endorsement towards the use of DNN as a tsunami hazard assessment tool.

## 2 Model Formulation

This DNN inverse model primarily uses the forward model of FITTNUSS (Naruse & Abe, 2017) and the key feature of the new inverse model is that the model is implemented by the artificial neural network. The forward model calculates sediment transportation and deposition from the averaged flow velocity, the maximum flow depth and initial sediment concentration, along with these it produces spatial distribution of thickness and grain size composition which are used to train the DNN inverse model.

### 2.1 Forward Model

FITTNUSS forward model is used in the present inverse model framework. Here, we describe about brief review of FITTNUSS forward model, and the details are given in Naruse and Abe (2017). In the FITTNUSS model, shallow layer-averaged one-dimensional equations are used, which take the form:

$$\frac{\partial h}{\partial t} + \frac{\partial Uh}{\partial x} = 0, \quad (1)$$

$$\frac{\partial Uh}{\partial t} + \frac{\partial U^2 h}{\partial x} = ghS - \frac{1}{2}g \frac{\partial h^2}{\partial x} - u_*^2. \quad (2)$$

where  $t$  and  $x$  are considered as time and the bed-attached streamwise coordinate that is, transverse to the shoreline and is positive landward side. Here,  $h$  refers to the tsunami inundation depth, and  $U$  is the flow velocity. Gravitational acceleration is denoted as  $g$ ,  $S$  is the bed slope and  $u_*$  is the friction velocity.

Sediment conservation equation of tsunami is given by:

$$\frac{\partial C_i h}{\partial t} + \frac{\partial U C_i h}{\partial x} = w_{si}(F_i E_{si} - r_{0i} C_i). \quad (3)$$

In the above equation,  $C_i$  refers to the volume concentration in suspension of the  $i$ th grain size class. The parameters  $w_{si}$ ,  $E_{si}$ ,  $r_{0i}$ ,  $F_i$  represent settling velocity, sediment entrainment coefficient, ratio of near-bed to layer-averaged concentration of the  $i$ th grain size class and volumetric fraction of sediment particles in the bed surface active layer above the substrate (Hirano, 1971). Closure equation for the above-mentioned equations are friction velocity ( $u_*$ ), Thickness of active layer ( $L_a$ ) (Yoshikawa & Watanabe, 2008), Shield's

dimensionless shear stress ( $\tau_{*m}$ ), settling velocity ( $w_{si}$ ) (Dietrich, 1982), sediment entrainment coefficient ( $E_{si}$ ) (Rijn, 1984), correction of damping effects ( $\psi_i$ ) (Rijn, 1984). For the sedimentation of Tsunamis, Exner equation of bed sediment continuity is used:

$$\frac{\partial \eta_i}{\partial t} = \frac{1}{1 - \lambda_p} w_{si} (r_{0i} C_i - F_i E_{si}). \quad (4)$$

Here  $\eta_i$  refers to volume per unit area (thickness) of sediments of  $i$ th grain size class which includes  $\lambda_p$ , porosity of the bed sediment  $\lambda_p$ . As a result of sedimentation, the grain size distribution in the active layer varies with time (Hirano, 1971), which is expressed as follows:

$$L_a \frac{\partial F_i}{\partial t} = \frac{\partial \eta_i}{\partial t} - F_i \frac{\partial \eta}{\partial t} \quad (5)$$

Thus, the rate of total sedimentation is:

$$\frac{\partial \eta}{\partial t} = \sum \frac{\partial \eta_i}{\partial t}. \quad (6)$$

Equations from (4) to (6) were solved using two step Adams-bashforth scheme and predictor-corrector method. Finally, simplification of flow dynamics of tsunami has been done using the assumption proposed by (Soulsby et al., 2007), considering velocity of tsunami run-up flow as uniform and steady but flow depth varies with time, hence it proves the model as quasi-steady flow assumption. Simplified equation is as follows:

$$\frac{\partial C_i}{\partial t} + U \frac{\partial C_i}{\partial x} = \frac{R_w}{H(Ut - x)} \{w_{si} (F_i E_{si} - r_{0i} C_i)\}. \quad (7)$$

Besides these formulations, a transformed coordinate system (Crank, 1984) has been applied to equation number (7) to increase computational efficiency of the forward model. Implicit Euler method was used to solve the equation after applying coordinate transformation. The entire forward and inverse model were implemented using Python with libraries numpy and scipy.

## 2.2 Inverse Model

Although artificial neural networks have been mostly applied to learn observational data sets to construct predictive models (Ramirez et al., 2005), this study uses it for learn-

ing results of numerical simulation to construct an inverse model. Firstly, an artificial training data sets are created by repetition of the forward model calculation with random initial and boundary conditions. Then, the data set that is spatial distribution of grain-size composition (Figure 1) is given to an input layer of the NN. Nodes in the input layer receive values of volume-per-unit-area of each grain size class at spatial grids used in the forward model. Feed-forward calculation through several hidden layers is then performed, in which values at nodes were summated with weighting coefficients that are assigned on connections to nodes in the next layer, and the computed total input data passes through the activation functions to produce the net output. The number of hidden layers was set to maximize the model performance (S. Smith, 2013). Resulting from this feed-forward calculation, values provided from output nodes give estimates of hydraulic conditions of tsunamis that formed deposits. This procedure leads to training of the model followed by testing of model performance. The 20% of the artificial data are used to validate the model performance during training. If the model tends to over-learn, the selection of hyperparameters and the optimization method must be checked. After the model training is done, the model becomes ready to apply for natural data set; however, the model performed training based on artificial data with a definite spatial grid interval.

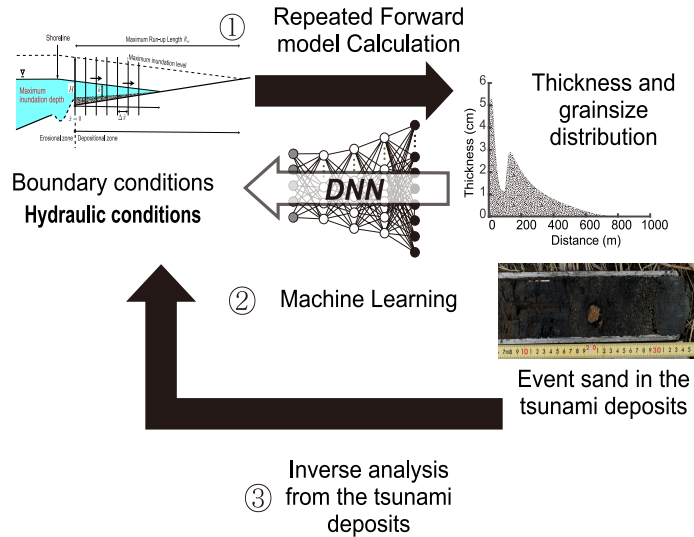


**Figure 1.** Flow diagram decribing the workflow of the DNN inverse model.

### 2.2.1 Procedures for training of the inverse model

Here, we describe the procedures for generating training data set and preprocessing. In present study, the forward model discretized grain-size distribution into 6 grain size classes, and number of spatial grids in the transformed coordinate was 50. The number of spatial grid size in fixed coordinates depends on the size of sampling window as mentioned before. It is important to determine the appropriate number of training data set produced by the forward model in order to improve the inverse model training (Jordan & Rumelhart, 1992). In this study, iteration of the forward model calculation was incrementally increased, and the relation between the number of training data sets and the performance of the inverse model was examined. Range of explored conditions in training data set is described later. The sampling window was then set to the artificial training data sets before starting the training of DNN, and the data only in the sampling window was used for the training. The reasons of necessity of this sampling window are (1) that thickness of collected samples at a distant location becomes too thin to measure precisely and predict computationally, and (2) the measurement transect cannot cover entire distribution of tsunami deposits in natural cases. Very thin and fine grained tsunami deposits in distal area may not be detected from the background soil, so that the region of analysis should be limited in relatively proximal area where coarse and thick-bedded deposits are distributed. Therefore, the specific window preferably at the proximal to middle part of the transect. As in the settings of our inverse model, the grid spacing has been kept constant which is 15 m in our model. The number of spatial grids in fixed coordinate varies according to the chosen interval the sampling window. After production of the training data set and extraction of sampling window, normalization of input and teacher values was performed, which is one of the most important process in training the neural network. As the input and teaching data have largely different range of values each other, so that the normalization of values is needed to remove computational biases towards a specific dimension of data (Bishop et al., 1995). In this case, the maximum inundation length has larger range of values while the values of concentration are very low, and thus raw values of teaching data may predict the inundation length preferentially and concentration values tend to be ignored. Therefore, both the input and teaching data in the artificial data set produced by the forward model were normalized before they were given to the inverse model. The input data (volume-per-unit-area of deposits) were normalized using the following equation:

$$X_{norm} = (X_{raw} - \min val_{X_{raw}}) / (\max val_{X_{raw}} - \min val_{X_{raw}}) \quad (8)$$

where  $X_{norm}$  and  $X_{raw}$  are normalized and original values of input data respectively.

$\min val_{X_{raw}}$  and  $\max val_{X_{raw}}$  denote minimum and maximum values of raw input data.

Similarly, the teaching data that was original conditions used in the forward model calculation was normalized by:

$$Y_{norm} = (Y_{raw} - \min val_{Y_{raw}}) / (\max val_{Y_{raw}} - \min val_{Y_{raw}}) \quad (9)$$

where  $Y_{norm}$  and  $Y_{raw}$  are normalized and original values of teaching data respectively.

$\min val_{Y_{raw}}$  and  $\max val_{Y_{raw}}$  denote minimum and maximum values of raw teaching data.

After the training, NN outputs the normalized values of hydraulic conditions, so that these values were converted to values in the original scale.

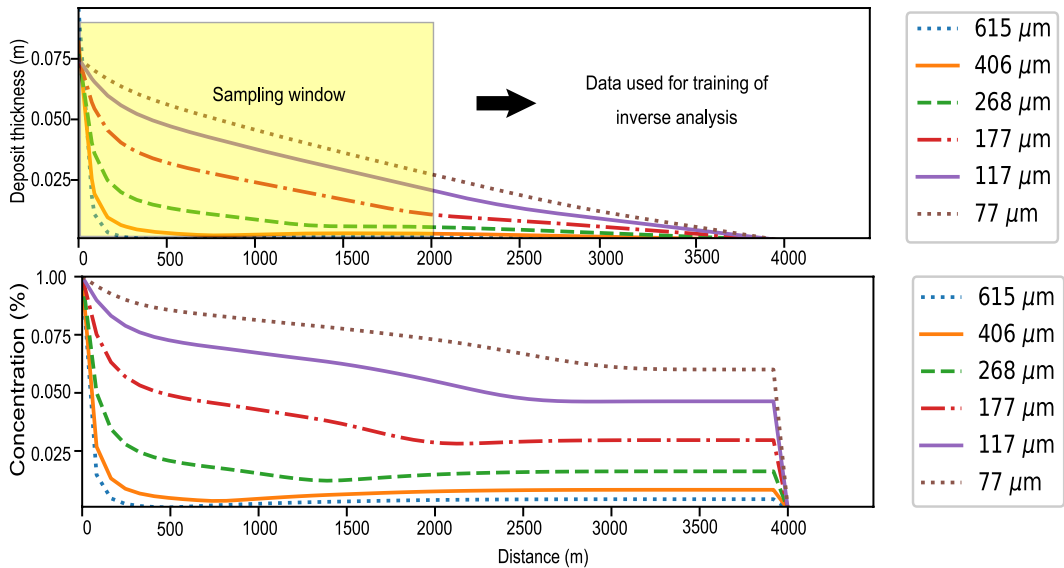


**Figure 2.** An example of forward model calculation and sampling window used for inverse analysis. (a) Spatial variation of volume-per-unit-area of each grain-size class of tsunami deposit calculated by forward model (b) Spatial variation of sediment concentration of each grain-size class in the run-up flow when the flow has reached the maximum inundation point. See text for details.

Then, the training and teaching were given to the NN for training. The overall neural network structure consists of three parts, the input layer, hidden layers, and output layer (Figure 3). In the inverse model, the input layer of neural network structure consists of input nodes where input values are values of volume-per-unit-area of each grain size class at spatial grids. Thus, number of input nodes becomes  $M \times N$  where  $M$  and  $N$  are total number of spatial grids and grain-size classes respectively. In this study, number of dense hidden layers was set to be three along with total 2500 nodes, and thus total number of layers was five (Figure 3). Here, the rectified linear activation function (ReLU) was used as an activation function that calculates the output value from the total net weighted inputs (Ian & Yoshua, 2016). ReLU is widely used function for this purpose (Macdonald & Cox, 1950). The drop out has been applied to the hidden layer for regularization of the NN (Srivastava et al., 2014). Results of feed-forward calculation of this NN during the training process were evaluated by the loss function (mean squared error) defined as follows:

$$J = \frac{1}{2} \sum \left( I_k^{fm} - I_k^{NN} \right)^2 \quad (10)$$

where  $I_k^{fm}$  is denoted as teaching data that are initial parameters used for producing in the training data and  $I_k^{NN}$  denotes predicted parameters. This loss function quantifies how close the NN was to an ideal inverse model. Values of this function were averaged over the entire data set (Patterson & Gibson, 2017). To minimize the loss function  $J$ , the back-propagation method with SGD (Stochastic Gradient Decent algorithm) was used to optimize the weight coefficients at links of the network (Patterson & Gibson, 2017). Nesterov momentum was used with SGD to speed up the computation and improve convergence (Sutskever et al., 2013). Although other optimizers such as AdaDelta, Adam or AdaMax (Patterson & Gibson, 2017), ), this optimizer was showing best performance in case of our model. This optimization process was repeated for prescribed times, and the training set was shuffled before splitting to batch chunks that were used for SGD optimization during each epoch.

In order to estimate how well the model has been trained without overfitting, validation was done with the validation data set that were also generated from the forward model calculation. Among the produced data sets, 80% and 20% of the data were used for training and validation respectively. Results of validation were used for tuning of hy-

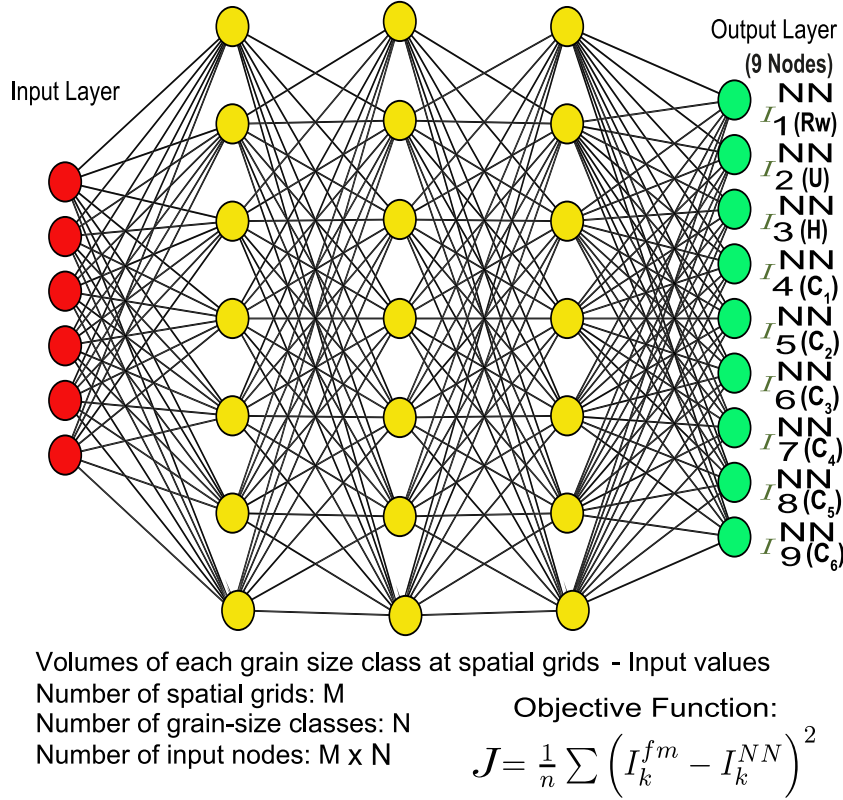


**Figure 3.** Neural network architecture for inverse model. Neural network structure includes one input and one output layer with 3 hidden layers, in total 5 layers. See text for details.

perparameters that are explained later. Finally, the performance of the model after the hyperparameter tuning was evaluated by test data sets that were unused data set during the training process.

In our model, there are several hyperparameters that should be specified for tuning of the training of NN. Tuned hyperparameters are: learning rates, batch size and momentum used in SGD, rates of drop out, number of hidden layers, types of activation function and number of epochs. The hyperparameters were chosen by trial and error in this study. The number of training data sets is also hyperparameter of the inverse model, and it was tested by changing number of repetition of the forward model calculation. The trained model can work on data set with a specific spatial grid in the fixed coordinate and grid spacing. In order to apply the inverse model to the natural data set in 1-d vectors, the collected samples must be fit into that fixed coordinate. Linear 1D interpola-

tion needed as it gets values at positions in between the data points which are joined by straight line segments (Bourke, 1999). Linear 1D interpolation has been applied to the natural data set in this case.

Apart from the training and validation data, 500 independent data have been kept aside for the testing of the inverse model. Therefore, after the model was trained, the model was applied to the test data sets to check its performance before applying to natural data sets. Correlation between teaching data in the test data set and the prediction of the model from the test data set was used to check how precise and accurate the inverse model prediction was. The residuals from the teaching data in the test data set plotted in the histogram to check how much the prediction from the test data set got deviated from the true initial conditions.

### **2.2.2 Uncertainty analysis of inversion results**

For error assessment of results of the inverse model, jackknife method was used in this study. This method estimates the standard error of predicted value of the model using a resampled population. Quenouille (1949) first introduced this resampling method (Nisbet et al., 2009).

The jackknife test is similar as the bootstrap method, but instead of random sampling of a data set, the inversion model works on each separate set of samples by omitting a single set of observations per iterations from total  $N$  observations. Inversions are carried out  $N$  times and the resulting ensemble of solutions were interrogated to a single estimate for each parameter. In short, it involves a leave-one-out strategy in a data set of  $N$  observations and the model works on the rest of the samples and gives results accordingly. Preferably,  $N-1$  observations were built on the data set as resampled data for the model. Farrell and Singh (2010) discussed the importance of jackknife method in survey sampling.

Here we briefly describe the jackknife uncertainty analysis. The estimate from a sample and the jackknife estimates are denoted as  $S$  and  $S^*$  respectively. The number of observations in the sample is  $N$  and the set of observations is denoted as  $\{X_1, \dots, X_n, \dots, X_N\}$ . The sample estimate of the parameter acts as a function of the observations in the sample (Abdi & Williams, 2010). The equation is:

$$S = f(X_1, \dots, X_n, \dots, X_N) \quad (11)$$

Let  $S_{-n}$  be the  $n$ -th partial prediction of the parameter, which is produced by the inverse model without the  $n$ th observation. The equation for the prediction  $S_{-n}$  is:

$$S_{-n} = f(X_1, \dots, X_{n-1}, X_{n+1}, \dots, X_N) \quad (12)$$

$S_n^*$  represents a pseudo value estimation of the  $n$ th observation. This parameter is defined as the difference between the estimates  $S$  obtained from the entire sample and the estimates  $S_{-n}$  obtained without the  $n$ th observation as follows:

$$S_n^* = NS - (N - 1)S_{-n} \quad (13)$$

The mean of the pseudo values are regarded as the jackknife estimate  $S^*$ . The equation for the jackknife estimate is:

$$S^* = S_{mean}^* = \frac{1}{N} \sum_n^N S_n^* \quad (14)$$

where  $S_{mean}^*$  is also the mean of the pseudo values. The variance of the pseudo values is denoted as  $\sigma_{JK}^{var}$  and the formula for the variance is:

$$\sigma_{JK}^{var} = \frac{\sum(S_n^* - S_{mean}^*)^2}{N - 1} \quad (15)$$

Finally, the jackknife standard error of the parameter estimate is denoted by  $\sigma_{JK}^{SE}$ , The formula for the jackknife standard error is:

$$\sigma_{JK}^{SE} = \sqrt{\frac{\sigma_{JK}^{var}}{N}} = \sqrt{\frac{\sum(S_n^* - S_{mean}^*)^2}{N(N - 1)}} \quad (16)$$

The confidence interval for this study has been computed with this jackknife standard error formula.

### 3 Results of training and test of the inverse model

The hyperparameters for training were set as follows. Among the hyperparameters used in SGD algorithm, the learning rate was set to be 0.02 and batch size was kept 32 for our models (Patterson & Gibson, 2017). Larger or smaller learning rates did not give improved results. Also, other batch sizes were tried in the training of the model, but the model was not improved. Selection of number of layers and number nodes were tested by increasing or decreasing layers or nodes, and finally three hidden layers with 2500 nodes were used in the models. Another hyperparameter is the rate of drop-out at each hidden layer, which was 50% in our model. Thus, during the training, 50% of the layer outputs that were randomly chosen kept inactive. This regularization process helps to reduce overfitting and increases the efficiency of the training (Srivastava et al., 2014). Finally, number of epochs in the training process, which means number of times that full data set has been passed the optimization calculation (J. Smith & Eli, 1995), were determined depending on the rates of the progress of the training (Figure 4). This is described in the following sections.

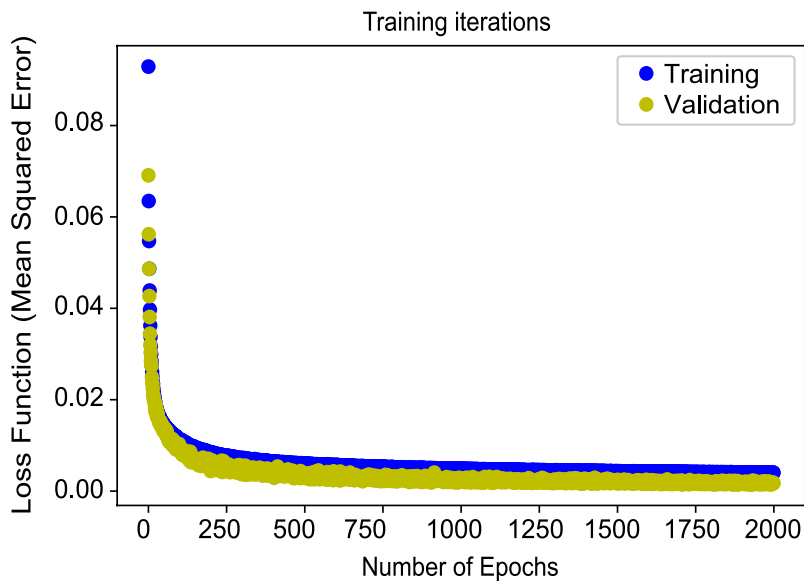


**Figure 4.** History of learning shown by variation of loss function (mean squared error). Both values of loss function for training and validation data sets decrease over 2000 epochs without any discrepancy, indicating that overlearning did not occur.

The input parameters for the inverse model were 9 that includes maximum inundation length flow velocity, maximum flow depth, and the sediment concentration of six grain size classes. The range of values for maximum inundation length was from 2500 to 4500 m, for flow velocity, maximum flow depth and sediment concentration used to generate training data sets were 1.5 m to 10 m/s, 1.5 m to 12 m and 0 to 2% respectively. The values of the loss function of training and validation at the first epoch were 0.0929 and 0.0691 for the training and validation data respectively. These values are based on the maximum records of tsunamis found in Mori et al. (2012), Nakajima and Koarai (2011), Foytong et al. (2013), B. E. Jaffe et al. (2012).

The values of the loss function of training and validation at the first epoch were 0.0929 and 0.0691 for the training and validation data respectively. The value of the loss function dropped less than 0.01 after 200 epochs. The present model converged reasonably over the 2000 epochs for both training and validation performance which remained in unison and equivalent rapidly within short period of time. Moreover, the plot for the loss function was smooth and there was no anomalous oscillation. The last and lowest loss function at the final epoch was 0.0040 for training data sets and was 0.0018 for the validation data sets. The sampling window was set from 0 to 2000 m in this training and the following tests (Figure 2).

For the current inverse models, the forward model was calculated repeatedly from 500 to 4500 iteration, and it showed the best result with 4500 repetitive calculation of forward model (Figure 5). Figure 5 plotted relation between number of training data and loss function of validation data set. The loss value of validation data set decreases with increasing number of training data, showing concave-up shape. When the number of training data set was 500, the loss function was higher but for the loss function eventually dropped drastically after 1500 training data sets. The loss function attained its minimum value after 3500 as the loss function did not change much after 3500 training data sets. Thus, it was suggested that the number of training data sets should be above 3500. The number of training data sets which is 4500 for certainty.

After the training of the model, the prediction results of the inverse model from the test data sets plotted against the original conditions used for producing the test data sets. Figure 6(a-i) shows that the 9 predicted initial conditions from the artificial test data sets were distributed around the 1:1 line in the graph, indicating that the test re-

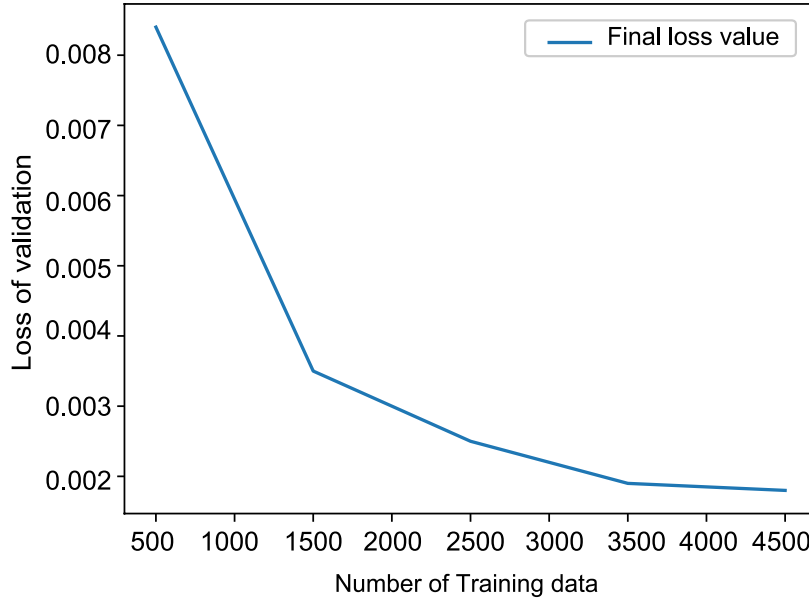


**Figure 5.** Relation between loss function of validation and number of training data sets chosen for inverse model. Result of training improved as number of training data sets increased, whereas it varied little after 4000.

sults show correlation with the true initial conditions. Also, the residuals of predicted parameters from the true initial conditions were plotted on a histogram to show distribution of deviation of the test results from the original conditions.

Figure 7(a-i) shows that deviation of predicted parameters from the original values were distributed in relatively narrow range without large biases from the true conditions except for the maximum flow depth. Only the maximum flow depth was slightly biased. Judging from the scatter diagram (Figure 7), the values of the predicted maximum flow depth were  $\sim 0.5$  m lower than the original value.

#### 4 Result of application to the 2011 Tohoku-Oki Tsunami deposit

The model was applied to the 2011 Tohoku -Oki Tsunami deposits distributed around Sendai plain for evaluation of the models. This region was extensively surveyed for hazard evaluation as well as tsunami deposits (Naruse & Abe, 2017; Abe et al., 2012), so that the large amounts of field data are available for evaluating the inverse models. Here, in this study, the same field data which was used also in FITTNUSS model (Naruse &

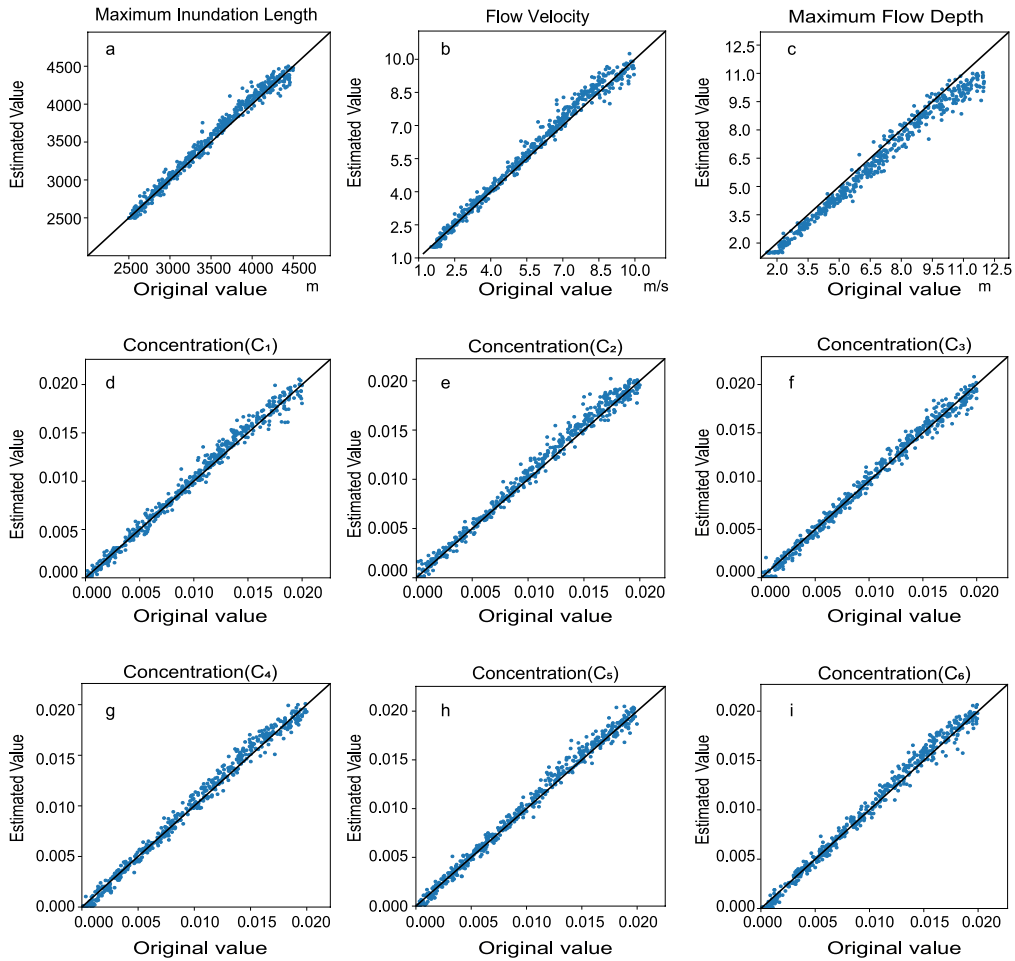


**Figure 6.** Performance of the model checked with artificial test data sets. Values estimated by the inverse model were plotted against the original values used for production of the test data sets. Solid lines indicating 1:1 relation suggest precise estimation. See details in the text.

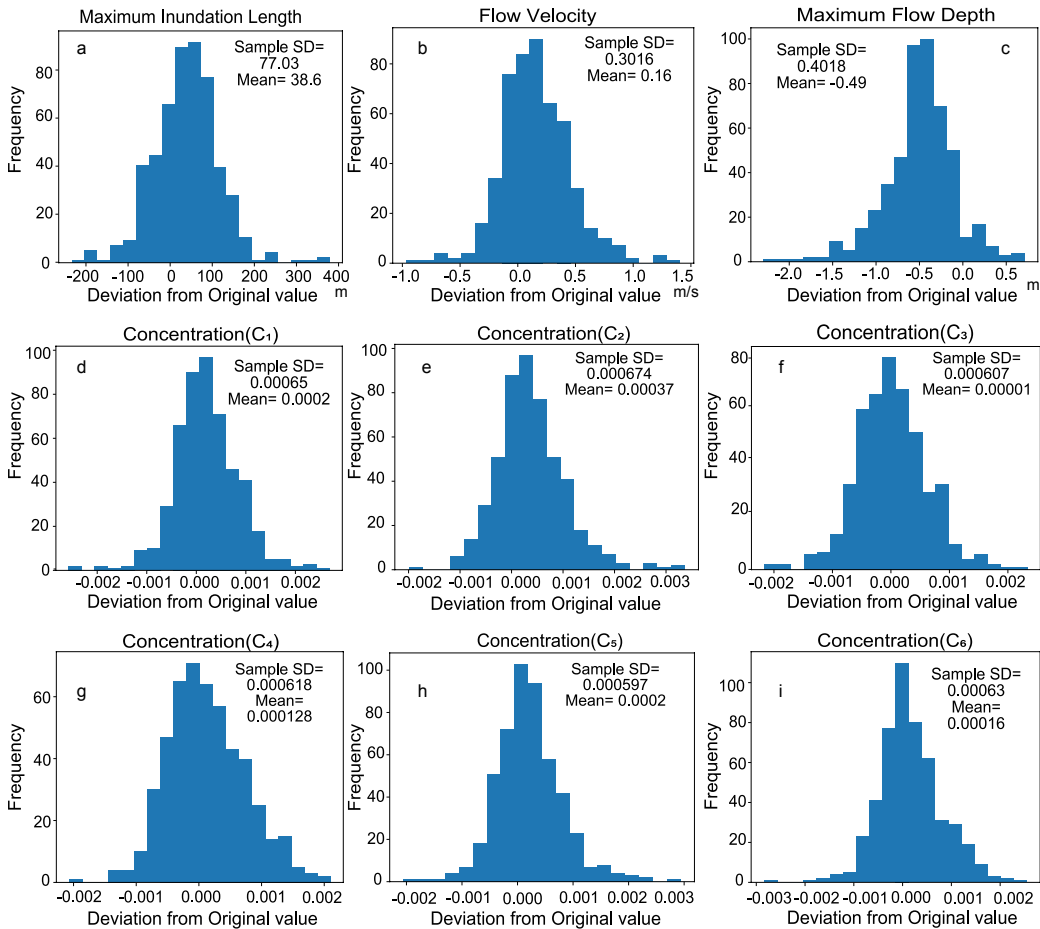


**Figure 7.** Histograms showing the deviation of predicted results from the original values of artificial test data sets.

Abe, 2017), and therefore the inversion methodology can be compared with the previous study.

#### 4.1 Field description and settings for inverse analysis

Here, we briefly state the field sampling method of measured data. The field work for this tsunami deposit was conducted soon after the tsunami event in June 2011 (Naruse & Abe, 2017) and details are given in Abe et al. (2012) and Naruse and Abe (2017). The study area (Figure 8) mainly consists of a long sandy beach, high onshore seawall, aeolian sand dune, coastal forest and long flat rice paddy field successively towards landward side (Naruse & Abe, 2017). The deposit was sampled every 50–100 m and 26 sites in total along the transect. The thickness of tsunami sand and mud layers ranged from 0.1 cm to 34 cm. Grain size analysis of the tsunami deposit showed that the tsunami sand was composed mostly of medium sand with small presence of fine and very fine sand (Naruse & Abe, 2017). Measured grain size distributions were then discretized to six grain size classes (Figure 9), while the previous FITTNUSS model employed four grain size classes (Naruse & Abe, 2017). The representative diameters of grain-size classes were 615, 406, 286, 177, 117 and 77  $\mu\text{m}$  respectively.

The parameters estimated by the inverse model such as the flow velocity were verified by comparing with data taken from the aerial videos and the observation in Sendai plain (Hayashi & Koshimura, 2013; Mori et al., 2012). Although it is difficult to assess sediment concentration data from the direct field observation, Goto et al. (2014) roughly estimated the sediment concentration in the tsunami inundation flow from the ratio between deposit thickness and flow height. We compared our reconstruction of the sediment concentration with their results.

#### 4.2 Determination of length of sampling window

In this case, sampling window was set from 0 to 2000 m along the transect. Although the total distance of the transect for collecting samples were around 3000 m, the measured bed thickness was very thin (several millimeters) and exhibited large fluctuation in the distal region (2000 to 3000 m) (Figure 12). Therefore, 2000 m long sampling window was extracted from the whole sampling distance which is 3000 m. This size of sampling window was also used for training of the inverse model. For this situation, the num-

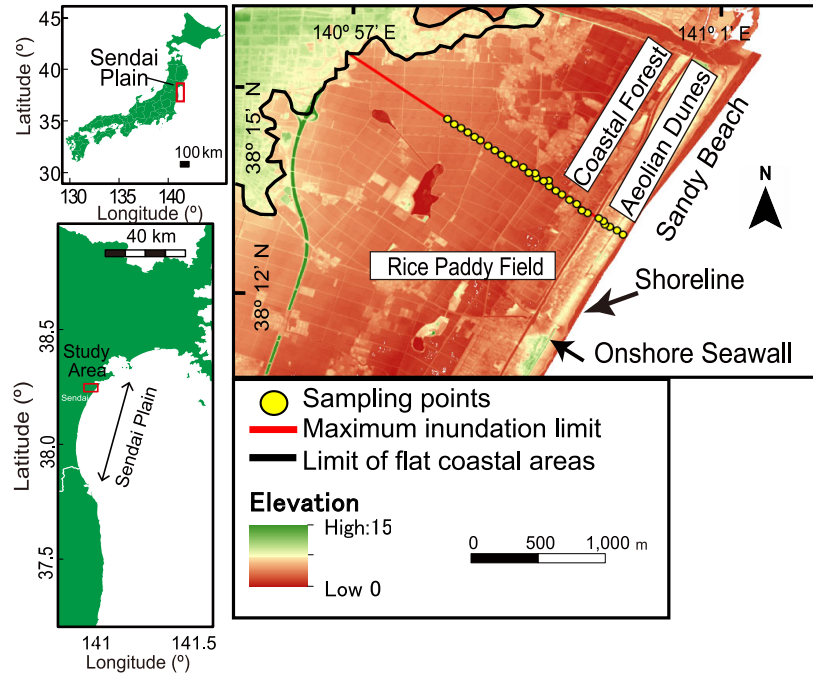


**Figure 8.** Location of the survey transect and sampling points on Sendai plain. The location of the surveyed transect is shown in topographic map of the study area. The 4 km long transect was situated transverse to the shoreline, and the tsunami deposit was sampled at the 27 locations along the transect (Naruse & Abe, 2017).

ber of spatial grids used for inversion was 133 because the grid spacing in fixed coordinates was 15 m. Selection of this size of the sampling window was checked by comparing with results using different sampling windows, suggesting that 2000 m is the best for obtaining stable results. Figure 9 shows the fluctuations of jackknife standard error estimation of parameters depending on the sampling window sizes. Most of parameters such as flow velocity and the concentrations exhibited trend to decrease their estimation errors as the length of the sampling window increases. Especially, the jackknife error of the flow velocity decreased largely above 1000 m in length. The estimates of the maximum inundation length show large errors but it dropped suddenly at around 2500 m. In contrast, the error of the maximum flow depth increased above 2000 m. Hence, it was decided that the size of the sampling window was set to be 2000 m. It should be noted that computation result for maximum inundation length was unstable at this selection.

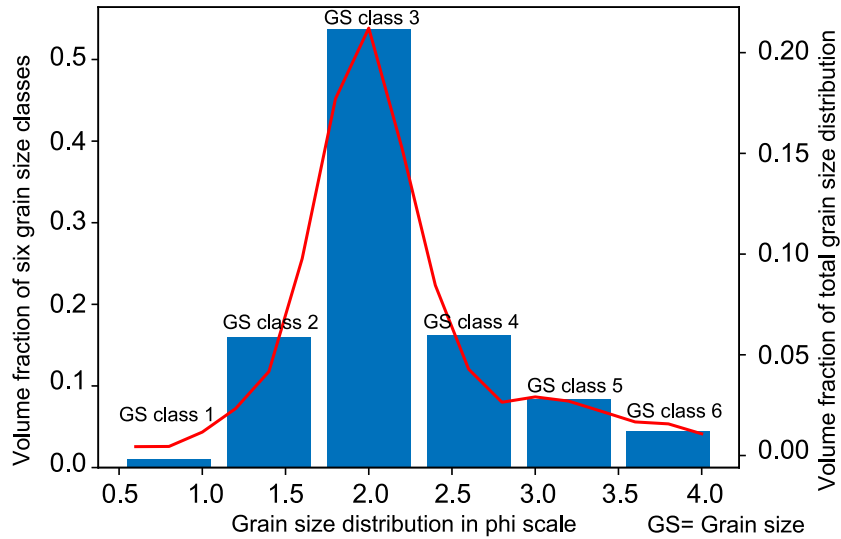


**Figure 9.** Total grain size distribution of tsunami deposit in Sendai plain and discretized fraction of sediment in six grain size classes.

#### 4.3 Result of inversion

The inverse model reconstructed the flow conditions of tsunamis from the deposit of 2011 Tohoku-Oki Tsunami in Sendai plain. The model estimated flow parameters close to observed values.

Table 1 shows the predicted hydraulic conditions of 2011 Tohoku-Oki Tsunami of Sendai plain. The predicted result of flow velocity was around 5.4 m/s with a range of uncertainty  $\pm 0.140$  m /sec using jackknife standard error calculation with 95% confidence interval (Figure 11b). The value of the maximum flow depth was around 4.11 m ( $\pm 0.152$  m uncertainty using Jack-knife standard error calculation (Figure 11c) with 95% confidence interval).

The reconstructed total sediment concentration over six grain-size classes was 5.08%. The estimated value of the sediment concentration of each grain-size class ranged from 0.04% to 2.19% (Figure 11d-11i).

The model predicted the maximum inundation length of the tsunami from the deposit, and the result was around 4045 m with  $\pm 121.17$  m jackknife standard error with 95% confidence interval (Figure 11a). Actual inundation length was 4020 m (Naruse & Abe, 2017), which is consistent with the reconstructed value.

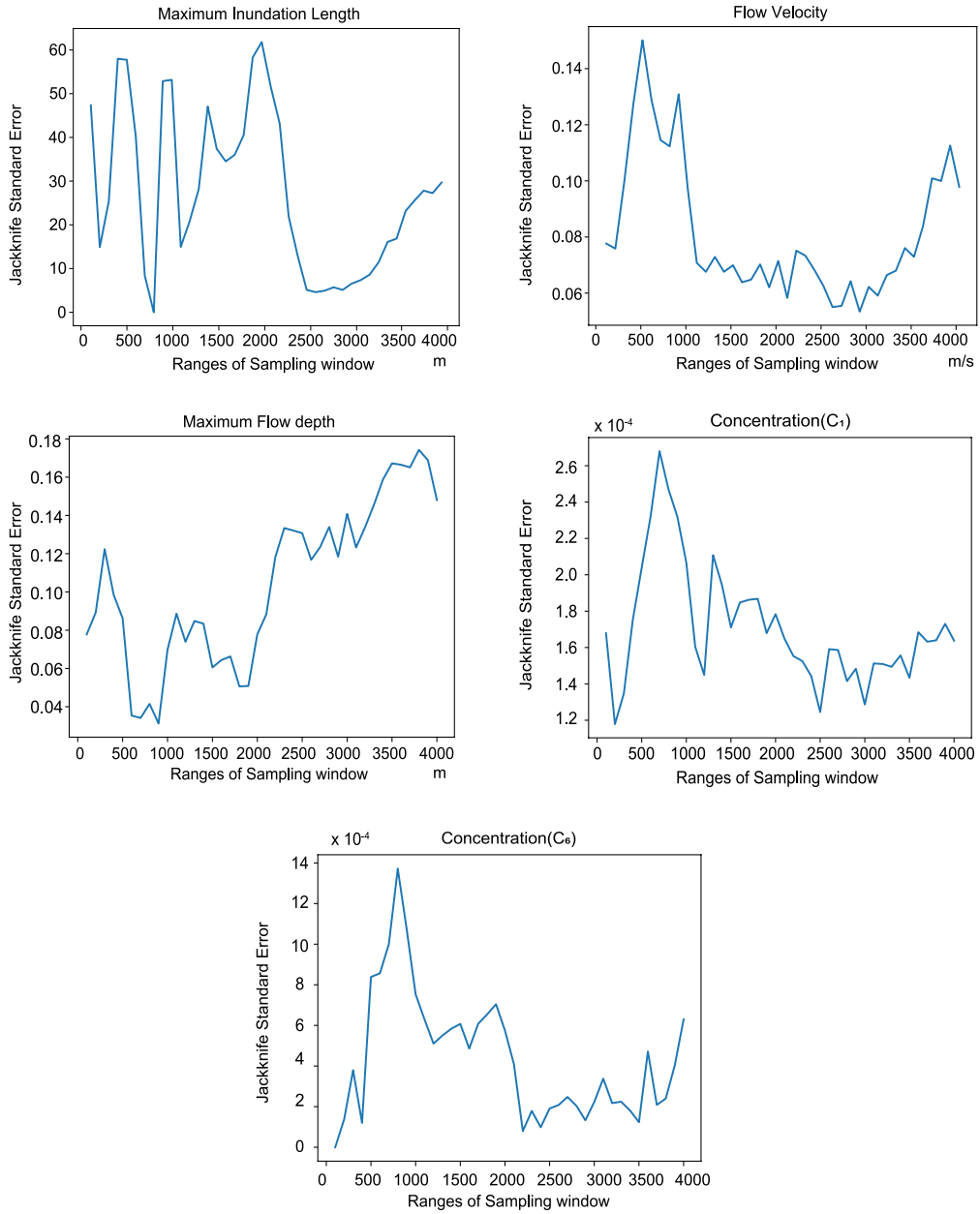


**Figure 10.** Variation of jackknife standard error with changing distance of sampling window

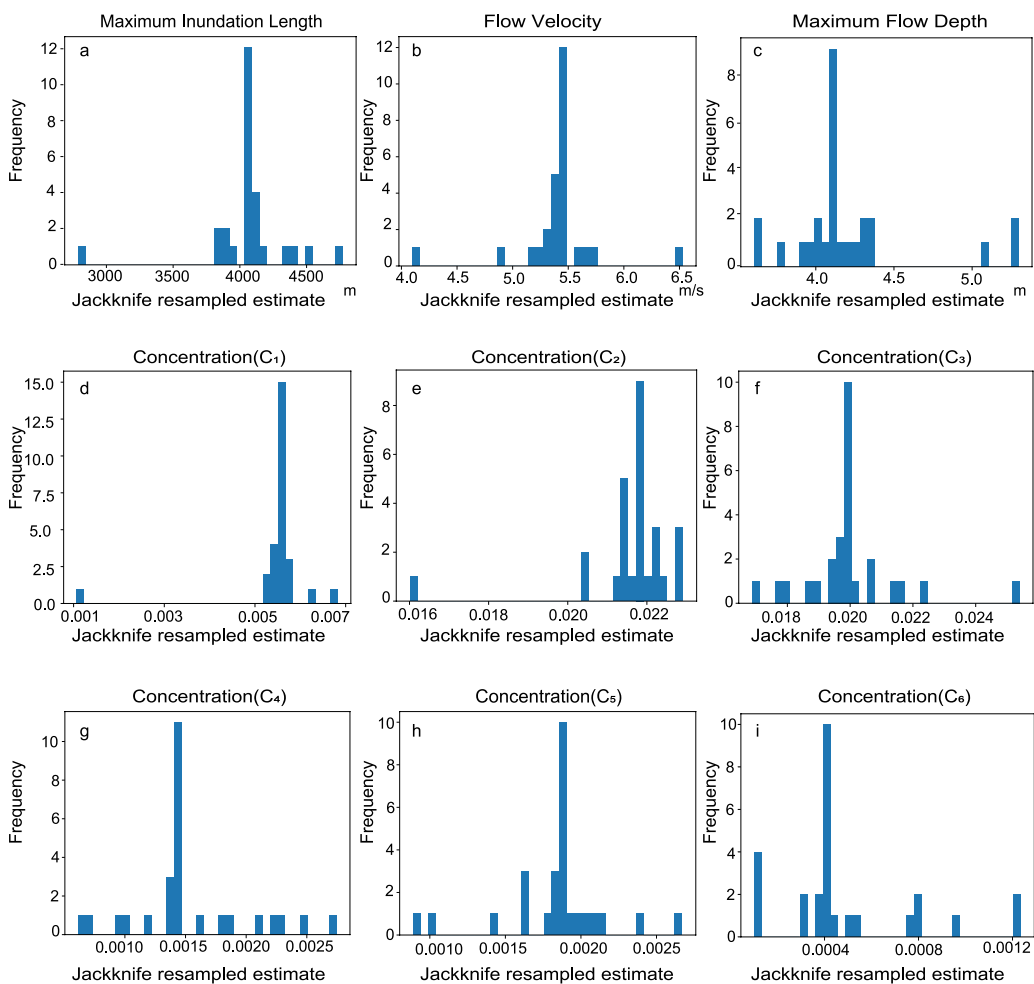


**Figure 11.** Jackknife estimates for the results predicted by the inverse model to check uncertainty of the model

**Table 1.** Predicted results by inverse model applied to 2011 Tohoku-Oki Tsunami deposit data obtained from Sendai plain

Name of the Parameters	Predicted Results	Confidence Interval (95%)
Maximum Inundation Length	4045 m	± 121.17 m
Flow Velocity	5.4 m/sec	± 0.140 m/sec
Maximum Flow Depth	4.11 m	± 0.152 m
Concentration of $C_1$ (615 $\mu\text{m}$ )	0.55%	± 0.034%
Concentration of $C_2$ (406 $\mu\text{m}$ )	2.19%	± 0.048%
Concentration of $C_3$ (268 $\mu\text{m}$ )	1.98%	± 0.058%
Concentration of $C_4$ (177 $\mu\text{m}$ )	0.14%	± 0.018 %
Concentration of $C_5$ (117 $\mu\text{m}$ )	0.18%	± 0.012%
Concentration of $C_6$ (77 $\mu\text{m}$ )	0.04%	± 0.0011%

For error assessment of model results, jackknife method was used. This method estimates the standard error and variance from a large population. Nisbet et al. (2009) first introduced this resampling method.

Finally, using the reconstructed initial conditions of the tsunami, the forward model calculated the spatial distribution of thickness and grain-size composition in order to compare with measured distribution. Figure 12 exhibits the thickness and grain-size distribution with distance for measured data and simulated results. The measured values of volume-per-unit-area for each grain size class were conformable with the simulated results except for the finest grain size class at which the predicted values were larger than the actual measurements.

## 5 Discussion

### 5.1 Tests of inverse models

The tests of the inverse models using the artificial data sets of tsunami deposits exhibited that the models built by neural networks can predict the flow velocity and the concentration of six grain-size classes, maximum inundation length precisely. The scatter diagram of predicted parameters against true conditions indicates excellent correla-

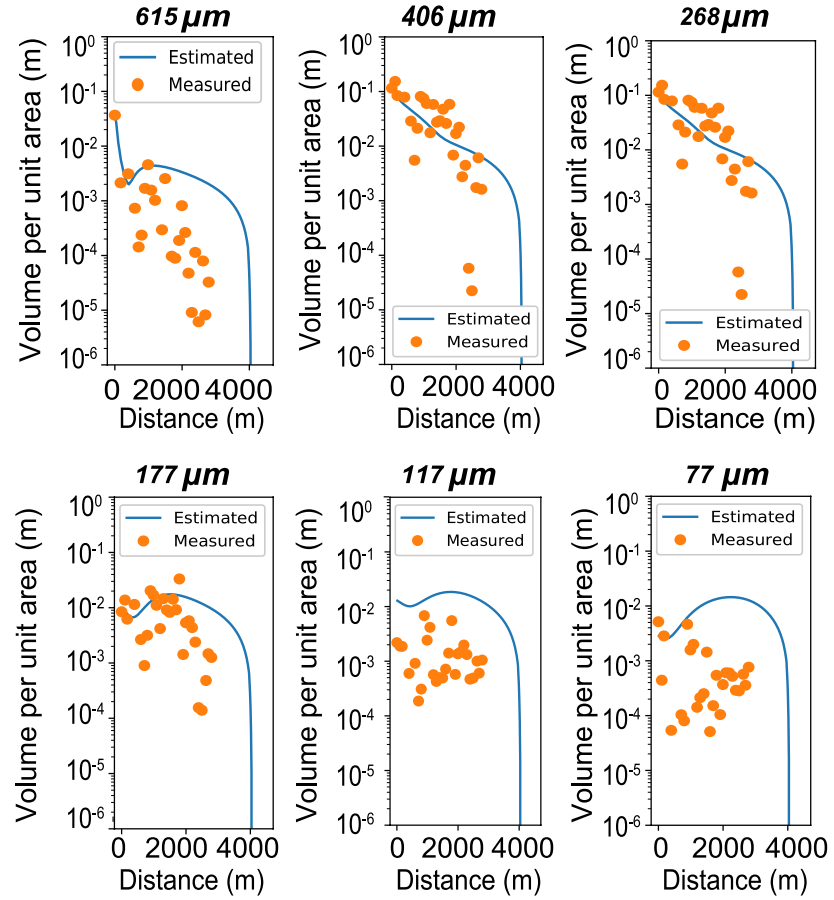


**Figure 12.** Spatial variation of thickness of the tsunami deposit. Spatial distribution of volumes-per-unit-area of six grain size classes was exhibited. The solid circles are values measured by Naruse and Abe (2017), and the lines indicate results of the forward model calculation using predicted parameters by the inverse model.

tion (Figure 6). For example,  $2\sigma$  of the estimation error of the maximum inundation length was 121.17 m, and the range of true values was 2500–4500 m (Figure 11). Thus, the precision of estimates is only the order of  $\sim 5\%$ . More importantly, there was no large deviation of mode of predicted values from true conditions except for the maximum flow depth. Especially in cases of estimates of sediment concentration, mean of the estimation errors ranges within  $1.0 \times 10^{-3}$ . These lines of results imply that the prediction of the inverse model is precise and accurate.

However, the model tends to estimate  $\sim 0.5$  m higher values for the maximum flow depth. As a result, while the deviation of the predicted values from the original values

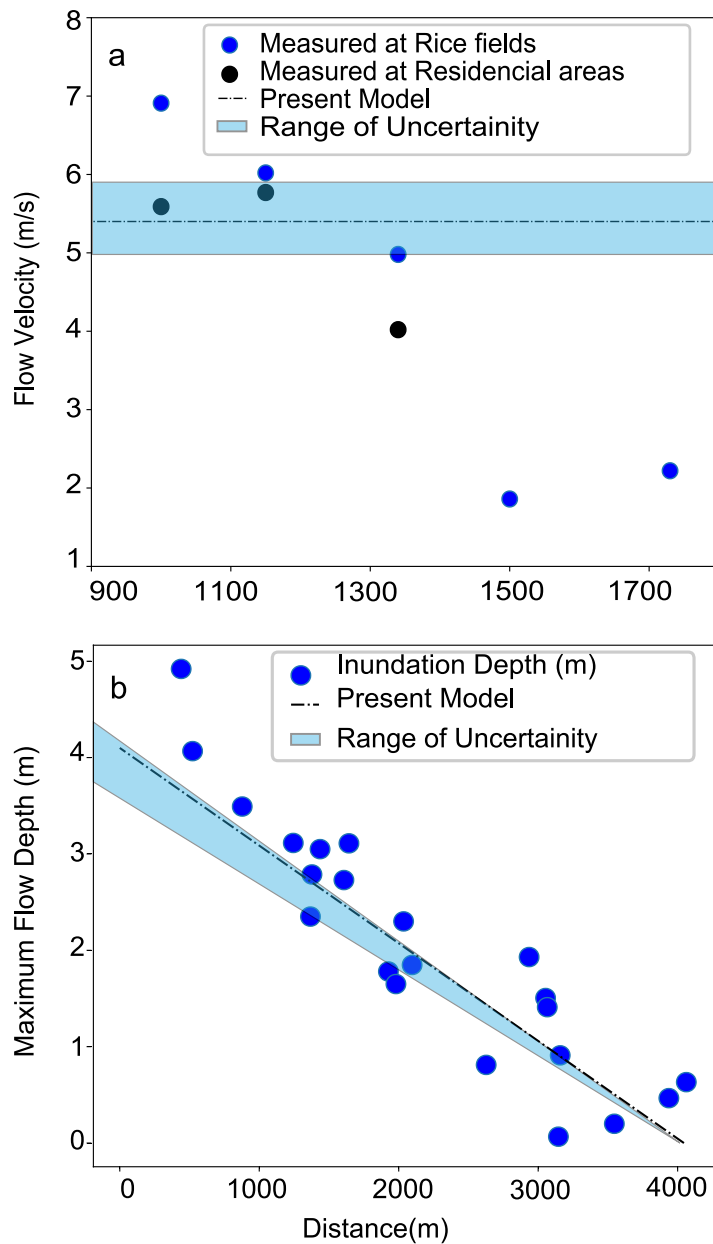


**Figure 13.** Comparison between field observation and results of inverse analysis of 2011 Tohoku-Oki Tsunami. The solid dots are measured values by field observation, and the lines are results of the inverse analysis of this study. (a) Velocity of run-up flow of the 2011 Tohoku-Oki tsunami on Sendai plain. (b) Maximum flow depth of 2011 Tohoku-Oki Tsunami on Sendai plain. Values measured from the aerial videos are indicated by the solid and open circles (Hayashi & Koshimura, 2013), and the results of the inverse analysis are shown by the lines

regarding to the maximum flow depth plotted in the histogram, the distribution of the deviation shows positive skewness and the mode value was about 0.5 m towards negative side. Despite the skewness, it is possible to correct the final result of the maximum flow depth by adding 0.5 m with the final reconstructed value from original field data.

## 5.2 Reconstruction of the flow parameters of the 2011 Tohoku-Oki Tsunami

After applying the inverse models to the 2011 Tohoku-Oki Tsunami, predicted results of the flow velocity and the inundation depth were close to the values observed by the aerial video and field measurements (Figure 13), implying the effectiveness of the proposed method to apply the actual tsunami deposits.

Figure 13 shows that averaged value of the observed inundating flow velocity of 2011 Tohoku-Oki Tsunami ranged from 4.8 to 5.8 m/s, and the reconstructed values are in this range.

The predicted inundation length was 4045 m which is very close to the original maximum inundation length which was around 4020 m. Furthermore, the model predicted concentration of six grain size classes satisfactorily. The range of estimated concentration for each grain-size class was 0.04–2.19 vol.%, and the total concentration was 5.08 vol.%. There has been no direct observation of sediment concentration in the inundating tsunami flows, so that it is impossible to compare the reconstruction with the actual observation. Goto et al. (2014) estimated the sediment concentration of the 2011 Tohoku-Oki Tsunami as roughly 2 vol.% from the ratio between thickness of tsunami deposits and the inundation depth. This estimate is smaller than the predicted values in this study. However, from the turbid water remained in the box after the tsunami, Arikawa (2019) recently reported that the tsunami flow reached  $1,130 \text{ kg/m}^3$  in density that corresponds to  $\sim 6$  vol.%, which is close to the prediction by the inverse models proposed in this study.

The predicted results for the maximum flow depth were also very close to the observed maximum flow depth from field data (Figure 13). The model predicted 4.11 m that approximates the observed values well. Uncertainty analysis by jackknife method indicated that the error of estimates ranges from 3.8 m to 4.4 m, which is reasonably narrow as an assessment of magnitude of the tsunami. However, considering reconstruction bias of the maximum flow depth that was detected when the inverse models were tested by the artificial data, 0.5 m should be added to the maximum flow depth predicted by

the inverse models (Figure 11c). Thus, the reconstructed values by the model may be corrected to be 4.6 m, which is more accurate with the observed data set.

### 5.3 Comparison with existing models

In the present study, we described about the use of deep learning neural network as an inversion technique with modified FITTNUSS forward model to perceive the initial hydraulic condition from the tsunami deposit. Large advantages of this new methodology are (1) that it can employ realistic forward model than previous, and (2) the performance of the inverse model can be tested before the application to actual deposits by using test artificial data sets. In addition, (3) it is possible to conduct the uncertainty analysis of inversion with the resampling method due to that computational efficiency of the model.

Firstly, (1) the DNN inverse model can employ the forward model that is computationally expensive. The new inverse model requires only the limited number of the iteration of the forward model calculation for production of the training data sets, and this iteration can be completely parallelized. Calculation of the production of each training data set is independent. In contrast, previous inverse models including FITTNUSS model (Naruse & Abe, 2017) employed the optimization method (e.g. L-BFGS) in which the forward model calculation depends on the result of previous iteration, so that this trial and error procedures cannot be parallelized. It was time consuming to obtain the best solution and was difficult to improve the computational efficiency in previous methodology. Therefore, previous inverse model only employed the largely abridged forward models such as the “moving-settling tube” (Soulsby et al., 2007) or sudden settling from equilibrium uniform flows (B. E. Jaffe & Gelfenbuam, 2007). Recent inverse model TSUFLIND (Tang et al., 2018; Tang & Weiss, 2015) also employed similar simplified assumption probably because of this computational load problem. The new inverse model diminishes this limitation on the forward model, so that it can potentially employ fully hydrodynamic models as the forward model.

Secondly, (2) the inverse model proposed here can be tested prior to the actual analysis because each inversion (i.e. feed-forward calculation of NN) finishes instantaneously in this method. In previous methods such as FITTNUSS, each inversion takes longer time so that it was not realistic to iterate inversion several hundred times for testing the per-

formance of the model. In addition, (3) modern statistical uncertainty analysis requires resampling procedures in which the iteration of inversion is also needed. Therefore, Jackknife uncertainty analysis was possible to apply in case of DNN inversion in this study, but FITTNUSS or other methods are difficult to provide error range of estimates in realistic time period.

## 6 Limitation and scope of improvement

The present model shows promising results, but reliability of this model needs to be validated by using more field data. Options and hyperparameters for inversion such as the sampling window size can be tested in other examples of modern tsunami deposits with known flow parameters. Furthermore, we need to apply it to tsunami deposits in Tohoku and other regions along with ancient tsunami deposits in order to scrutinize the present model in a befitting manner and to make a robust model that can be used in the relevance of hazard evaluation.

In addition, the model still has some limitation in the applicability and accuracy. For example, reconstructed values of the maximum flow depth was biased -0.5 m, and the cause of this bias is unknown. However, for deciphering other parameters like maximum inundation length, flow velocity, concentration etc., this model showed satisfactory results for any scale of tsunamis. Currently this model can only be applied for the flat coastal areas and does not incorporate steeply sloping surface or topographically complicated regions. Nevertheless, these limitations can be solved by further modification of the forward model because the DNN inversion model can potentially incorporate complete hydrodynamic models as the forward model.

## 7 Conclusion

The present new model uses artificial neural network to derive hydraulic conditions of tsunami. It successfully reconstructed the flow conditions including the maximum inundation length, flow velocity, the maximum flow depth, concentrations from artificial tsunami deposits produced by the forward model as well as the natural tsunami deposits of 2011 Tohoku-Oki Tsunami. Reconstructed the flow velocity and the maximum depth were 5.4 m/sec and 4.11 m respectively, which are in the range of observed values of the tsunami. Uncertainty of the results has been checked with jackknife method which also shows that the model yielding results do not comprise large ranges of data. Thus, this

model is expected to successfully reconstruct the flow conditions of modern and ancient tsunamis in future studies.

### Acknowledgments

The implementation of the DNN inverse model is available as the open source software online (at <https://github.com>). We express our sincere gratitude to Prof. Takao Ubukata and other researchers in the biosphere study group of Kyoto University for their valuable suggestions. We thank Dr. Tomoya Abe for proving the post-tsunami DEM data for the formulation of the map and his support. The authors thank Kyoto University for providing all the facilities and Ministry of Education, Culture, Sports, Science and Technology, Japan for providing the permission and scholarship to carry out this collaborative research in Japan.

### References

- Abdi, H., & Williams, L. J. (2010). Jackknife. *Encyclopedia of research design*, 2.
- Abe, T., Goto, K., & Sugawara, D. (2012). Relationship between the maximum extent of tsunami sand and the inundation limit of the 2011 tohoku-oki tsunami on the sendai plain, japan. *Sedimentary Geology*, 282, 142–150.
- Arikawa, T. (2019). *The threat of the “black tsunami” revealed*. <https://www.nhk.or.jp/special/plus/articles/20190314/index.html>. (Accessed: 2019-04-12)
- Bishop, C. M., et al. (1995). *Neural networks for pattern recognition*. Oxford university press.
- Bourke, P. (1999). Interpolation methods. *Miscellaneous: projection, modelling, rendering.(1)*.
- Costa, P. J., Andrade, C., Cascalho, J., Dawson, A. G., Freitas, M. C., Paris, R., & Dawson, S. (2015). Onshore tsunami sediment transport mechanisms inferred from heavy mineral assemblages. *The Holocene*, 25(5), 795–809.
- Crank, J. (1984). *Free and moving boundary problems*. Clarendon press Oxford.
- Dietrich, W. E. (1982). Settling velocity of natural particles. *Water resources research*, 18(6), 1615–1626.
- Farrell, P. J., & Singh, S. (2010). Some contributions to jackknifing two-phase sampling estimators. *Survey Methodology*, 36(1), 57–68.

- Foytong, P., Ruanggrassamee, A., Shoji, G., Hiraki, Y., & Ezura, Y. (2013). Analysis of tsunami flow velocities during the march 2011 tohoku, japan, tsunami. *Earthquake Spectra*, 29(s1), S161–S181.
- Ganti, V., Chu, Z., Lamb, M. P., Nittrouer, J. A., & Parker, G. (2014). Testing morphodynamic controls on the location and frequency of river avulsions on fans versus deltas: Huanghe (yellow river), china. *Geophysical Research Letters*, 41(22), 7882–7890.
- Ghobarah, A., Saatcioglu, M., & Nistor, I. (2006). The impact of the 26 december 2004 earthquake and tsunami on structures and infrastructure. *Engineering structures*, 28(2), 312–326.
- Goto, K., Hashimoto, K., Sugawara, D., Yanagisawa, H., & Abe, T. (2014). Spatial thickness variability of the 2011 Tohoku-oki tsunami deposits along the coastline of Sendai Bay. *Marine Geology*, 358, 38–48.
- Hayashi, S., & Koshimura, S. (2013). The 2011 tohoku tsunami flow velocity estimation by the aerial video analysis and numerical modeling. *Journal of Disaster Research*, 8(4), 561–572.
- Hirano, M. (1971). River bed degradation with armoring. *Proceedings of Japan Society of Civil Engineers*, 1971(195), 55–65.
- Ian, G., & Yoshua, B. (2016). *Deep learning (adaptive computation and machine learning)*. MIT Press, Cambridge.
- Imamura, F., Boret, S. P., Suppasri, A., & Muhari, A. (2019). Recent occurrences of serious tsunami damage and the future challenges of tsunami disaster risk reduction. *Progress in Disaster Science*, 1, 100009.
- Jaffe, B., Goto, K., Sugawara, D., Gelfenbaum, G., & La Selle, S. (2016). Uncertainty in tsunami sediment transport modeling. *Journal of Disaster Research*, 11(4), 647–661.
- Jaffe, B. E., & Gelfenbuam, G. (2007). A simple model for calculating tsunami flow speed from tsunami deposits. *Sedimentary Geology*, 200(3-4), 347–361.
- Jaffe, B. E., Goto, K., Sugawara, D., Richmond, B. M., Fujino, S., & Nishimura, Y. (2012). Flow speed estimated by inverse modeling of sandy tsunami deposits: results from the 11 march 2011 tsunami on the coastal plain near the sendai airport, honshu, japan. *Sedimentary Geology*, 282, 90–109.
- Jerolmack, D. J., & Paola, C. (2010). Shredding of environmental signals by sedi-

- ment transport. *Geophysical Research Letters*, 37(19).
- Johnson, J. P., Delbecq, K., & Kim, W. (2017). Predicting paleohydraulics from storm surge and tsunami deposits: Using experiments to improve inverse model accuracy. *Journal of Geophysical Research: Earth Surface*, 122(4), 760–781.
- Jordan, M. I., & Rumelhart, D. E. (1992). Forward models: Supervised learning with a distal teacher. *Cognitive science*, 16(3), 307–354.
- Lin, A., Ikuta, R., & Rao, G. (2012). Tsunami run-up associated with co-seismic thrust slip produced by the 2011 mw 9.0 off pacific coast of tohoku earthquake, japan. *Earth and Planetary Science Letters*, 337, 121–132.
- Macdonald, G., & Cox, D. (1950). The tsunami of april 1, 1946. bul!. scripps inst. *Oceanogr*, 5, 391–528.
- Madsen, O., Wright, L., Boon, J., & Chisholm, T. (1993). Wind stress, bed roughness and sediment suspension on the inner shelf during an extreme storm event. *Continental Shelf Research*, 13(11), 1303–1324.
- Moore, G., Bangs, N., Taira, A., Kuramoto, S., Pangborn, E., & Tobin, H. (2007). Three-dimensional splay fault geometry and implications for tsunami generation. *Science*, 318(5853), 1128–1131.
- Mori, N., Takahashi, T., & Group, . T. E. T. J. S. (2012). Nationwide post event survey and analysis of the 2011 tohoku earthquake tsunami. *Coastal Engineering Journal*, 54(1), 1250001–1.
- Nakajima, H., & Koarai, M. (2011). Assessment of tsunami flood situation from the great east japan earthquake. *Bull Geospatial Info Authority Japan*, 59, 55–66.
- Naruse, H., & Abe, T. (2017). Inverse tsunami flow modeling including nonequilibrium sediment transport, with application to deposits from the 2011 tohoku-oki tsunami. *Journal of Geophysical Research: Earth Surface*, 122(11), 2159–2182.
- Nisbet, R., Elder, J., & Miner, G. (2009). *Handbook of statistical analysis and data mining applications*. Academic Press.
- Patterson, J., & Gibson, A. (2017). *Deep learning: A practitioner's approach*. ”O'Reilly Media, Inc.”.
- Quenouille, M. (1949, 01). Approximate tests of correlation in time-series. *Journal of the Royal Statistical Society B*, 11, 68-84. doi: 10.1017/S0305004100025123

- Rijn, L. C. v. (1984). Sediment transport, part ii: suspended load transport. *Journal of hydraulic engineering*, 110(11), 1613–1641.
- Romano, M., Lioung, S.-Y., Vu, M. T., Zemskyy, P., Doan, C. D., Dao, M. H., & Tkalich, P. (2009). Artificial neural network for tsunami forecasting. *Journal of Asian Earth Sciences*, 36(1), 29–37.
- Saatcioglu, M., Ghobarah, A., & Nistor, I. (2005). Effects of the december 26, 2004 sumatra earthquake and tsunami on physical infrastructure. *ISET J. Earthq. Technol*, 42, 79–94.
- Smith, D., Foster, I. D., Long, D., & Shi, S. (2007). Reconstructing the pattern and depth of flow onshore in a palaeotsunami from associated deposits. *Sedimentary Geology*, 200(3-4), 362–371.
- Smith, J., & Eli, R. N. (1995). Neural-network models of rainfall-runoff process. *Journal of water resources planning and management*, 121(6), 499–508.
- Soulsby, R. L., Smith, D. E., & Ruffman, A. (2007). Reconstructing tsunami run-up from sedimentary characteristics—a simple mathematical model. In *Coastal sediments* (Vol. 7, pp. 1075–1088).
- Srivastava, N., Hinton, G., Krizhevsky, A., Sutskever, I., & Salakhutdinov, R. (2014). Dropout: a simple way to prevent neural networks from overfitting. *The journal of machine learning research*, 15(1), 1929–1958.
- Sugawara, D., Goto, K., & Jaffe, B. E. (2014). Numerical models of tsunami sediment transport—current understanding and future directions. *Marine Geology*, 352, 295–320.
- Sutskever, I., Martens, J., Dahl, G., & Hinton, G. (2013). On the importance of initialization and momentum in deep learning. In *International conference on machine learning* (pp. 1139–1147).
- Tang, H., Wang, J., Weiss, R., & Xiao, H. (2018). Tsuflind-enkf: Inversion of tsunami flow depth and flow speed from deposits with quantified uncertainties. *Marine Geology*, 396, 16–25.
- Tang, H., & Weiss, R. (2015). A model for tsunami flow inversion from deposits (tsuflind). *Marine geology*, 370, 55–62.
- Yoshikawa, Y., & Watanabe, Y. (2008). Examine of Manning's coefficient and the bed-load layer for one-dimensional calculation of bed variation. *Monthly Report of Civil Engineering Research Institute for Cold Region*, 662, 11–20.